Ponderomotive and resonant effects in the acceleration of particles by electromagnetic modes

I. Almansa*,[1] F.B. Russman†,[1] S. Marini‡,[2] E. Peter§,[1] G.I. de Oliveira ¶,[3] R. A. Cairns**,[4] and F.B. Rizzato††[1]

[1]*Instituto de Física, Universidade Federal do Rio Grande do Sul, Caixa Postal 15051, 91501-970 Porto Alegre, RS, Brasil*

[2]*LULI, Sorbonne Université, CNRS, École Polytechnique, CEA, Université Paris-Saclay, F-75252 Paris cedex 05, France*

[3]*Instituto de Física, Universidade Federal do Mato Grosso do Sul, Caixa Postal 549, 79070-900 Campo Grande, MS, Brasil*

[4]*School of Mathematics and Statistics, University of St Andrews, St Andrews, KY16 9SS, UK.*

In the present analysis we study the dynamics of charged particles under the action of slowly modulated electromagnetic carrier waves. With the use of a high-frequency laser mode along with a modulated static magnetic wiggler, we show that the ensuing total field effectively acts as a slowly modulated high-frequency beat-wave field typical of inverse free-electron laser schemes. This effective resulting field is capable of accelerating particles in much the same way as space-charge wake fields do in plasma accelerators, with the advantage of being more stable than plasma related methods. Acceleration occurs as particles transition from ponderomotive to resonant regimes, so we develop the ponderomotive formalism needed to examine this problem. The ponderomotive formalism includes terms that, although not discussed in the usual applications of the approximation, are nevertheless of crucial importance in the vicinity of resonant capture. The role of these terms is also briefly discussed in the context of generic laser-plasma interactions.

I. INTRODUCTION

Plasma based particle acceleration by electromagnetic waves has been a subject of interest and intense scrutiny for many years, since early works on both magnetised and unmagnetised configurations [1–6].

In a recent paper the interaction of charged particles with localised wave modes was analysed, with central focus on the transition from the ponderomotive to the resonant regimes of the interaction [7]. The model developed in the analysis described the dynamics of relativistic particles in the field of purely electrostatic modes acting as slowly modulated, high-frequency carriers.

A series of results obtained in the course of the investigation suggest that efficient particle acceleration can be achieved even from relatively small injection velocities, as a result of ponderomotive and resonant effects combined. The ponderomotive force can pull particles towards wave-particle resonant conditions, and the resonance itself provides the ultimate acceleration to close to the speed of light.

Proper electrostatic modes for acceleration can be obtained in plasmas in the form of plasma waves. Plasma waves propagate within a relatively wide spectrum of phase-velocities [8], but have zero group velocity in cold plasmas. This pair of conditions (wide velocity spectrum and zero group velocity) is what is needed to create a localised stationary envelope of a high-frequency carrier, which has been shown to be a convenient structure for acceleration.

Plasmas are, however, known to be unstable and not particularly amenable to external control. To circumvent this difficulty, it has been argued in the original work [7] that a similar effect could be obtained with use of an inverse free-electron laser (FEL) configuration, formed by properly modulated wiggler and laser modes [9–11]. The effective beat mode formed by the laser and wiggler fields would act similarly to the electric potential of the electrostatic mode to provide the longitudinal accelerating forces. The general motivation here, as mentioned earlier, is that since electromagnetic modes do not need a plasma environment, the overall scheme would be more stable and robust. The concept was briefly discussed, but not adequately explored.

The purpose of the present work is thus to investigate this alternative but similar accelerating scheme, with electromagnetic modes instead of the electrostatic mode. The formalism requires more of an involved procedure to obtain an accurate description of the ponderomotive regimes valid at larger field amplitudes. This will bring us to a relevant discussion on the problem of uphill acceleration of charged particles in ponderomotive effective potentials [12–15]. We shall see that uphill acceleration is always present as particles migrate from the ponderomotive to the resonant regime, at which point they jump to high-speeds due to resonant trapping.

In the following sections we introduce the model, derive a canonical averaging procedure for the ponderomotive regime, analyse the full problem including comparisons with the ponderomotive approximation, and finally draw our conclusions.

*ivanessa.almansa@ufrgs.br
†russman@ufrgs.br
‡marini@ufrgs.br
§peterpeter@uol.com.br
¶glaucius.oliveira@ufms.br
**rac@st-andrews.ac.uk
††rizzato@if.ufrgs.br

II. THE MODEL

The model to be investigated in the present paper consists of a relativistic particle interacting with a modulated wiggler and a constant amplitude laser field, both circularly polarized. The wiggler is taken as a static structure for simplicity, but extensions to general electromagnetic (laser) wigglers are expected to produce similar results. Since we consider fields with constant amplitudes, self-consistency and wave damping effects are not taken into account in the present analysis. These effects are recognized as noteworthy in dense, high-current circumstances [16] and shall be examined in future work.

The wiggler and the laser are respectively written in the form

$$\mathbf{A}_w = A_{w0}\, e^{-\frac{x^2}{2\sigma^2}} \left[\cos(\theta_w)\hat{\mathbf{y}} - \sin(\theta_w)\hat{\mathbf{z}}\right], \tag{1}$$

$$\mathbf{A}_l = A_{l0} \left[\cos(\theta_l)\hat{\mathbf{y}} + \sin(\theta_l)\hat{\mathbf{z}}\right], \tag{2}$$

where A_{w0} and A_{l0} are the wiggler and laser respective constant amplitudes, and where $\theta_l \equiv k_l x - \omega_l t$ and $\theta_w \equiv k_w x$ are the phases of the laser wave and the magnetic wiggler. As we shall see shortly, the chosen polarizations for the potentials are essential to create a single resonance with which efficiently accelerate particles. The presence of harmonics of the fields, for instance, would make it harder to achieve optimal acceleration. We also note that the laser is uniform but the wiggler exhibits a central hump of width $\sim \sigma$ which will be also essential to provide optimal conditions for acceleration. We shall take $\sigma \gg 1/k_{l,w}$ to comply with the slow modulational condition. The one-dimensional model for the potentials is chosen for simplicity and to show the agreement between theory and computational results. Despite its simplicity, the one-dimensional character of the potentials can be taken as a good approximation for three-dimensional settings if: (i) - one works with thin beams whose cross section is much smaller than the laser spot size, and (ii) - note as well that in relativistic beams the effective particle mass limits particle transverse excursions to paraxial regions where dependence of the magnetostatic wiggler on transverse coordinates is very small. Quick estimates indeed show that typical corrections to the wiggler field due to transverse effects, as for instance terms of the form $(k_w r_\perp)^2/8$ arising from expansions of Bessel functions [17], are much smaller than the unity and can be discarded under the present circumstances. Betatron oscillations are ignored under the same approximation.

Arbitrary modulations of both fields over length and time scales much greater than those associated with the wave could be introduced and the analysis carried through in exactly the same way.

From the fully dimensional relativistic Lagrangian

$$L = -mc^2\sqrt{1 - v^2/c^2} + (q/c)\,\mathbf{A}\cdot\mathbf{v}, \tag{3}$$

the canonical Hamiltonian can be obtained in the following dimensionless form

$$H = \gamma = \sqrt{1 + p_x^2/\alpha + A_{l,0}^2 + A_{w,0}^2 e^{-\frac{x^2}{\sigma^2}} + 2A_{l,0}A_{w,0}e^{-\frac{x^2}{2\sigma^2}}\cos(x-t)}. \tag{4}$$

In the above Eq. (4) we introduce $\sqrt{\alpha} \equiv \omega/c(k_l + k_w)$ as the dimensionless phase-velocity of the FEL traveling wave carrier mode, formed by the beat-like coupling of the wiggler and laser fields [18]. In addition, we adopt the following set of normalisations: $H/mc^2 \to H$, $\sqrt{\alpha}p_x/mc \to p_x$, $q\mathbf{A}/mc^2 \to \mathbf{A}$, $(k_l + k_w)(x, \sigma) \to (x, \sigma)$, and $\omega t \to t$, with m as the particle mass, q as its charge, c as the speed of light, and γ as the relativistic factor.

We note that due to the normalizations adopted, the particle velocity measured in units of $\alpha^{-1/2}$ is equal to the dimensional velocity normalized by the speed of light, $v_{x,dim}/c$; in other words, $v_{x,dim}/c = v_x\sqrt{\alpha}$, a relation that helps to shorten the notation in the coming discussion.

The Hamiltonian (4) is exact for the conditions of our analysis and one sees that it resembles the purely electrostatic version discussed in Refs. [7, 15]. Indeed, the effective 1D dynamics along the x-axis contains a slowly modulated high-frequency carrier term that can therefore trap and accelerate particles if proper resonant conditions are met. The resemblance becomes even more striking in regimes of low-amplitude fields, where after a Taylor expansion of Hamiltonian (4) the beat-wave field takes on the electrostatic-like shape of an additive potential.

One can start the analysis of slowly modulated high-frequency Hamiltonians of the form (4) with aid of a ponderomotive approach. The ponderomotive approximation, when valid, describes the dynamics in terms of time averaged (over high-frequencies) quantities, which leads to a simpler and often integrable formalism. It has been argued that a proper ponderomotive approximation, based on cycle-averaged Lagrangians, can be obtained as one replaces the radicand in expression (4) with its time average [12, 13]. In practical terms this procedure removes the time dependent beat. The resulting expression is accurate provided that the particle velocity keeps well away from the resonance ($\dot{x} = 1$) where the formalism breaks down and particles are captured by

the resonance. However, since the whole premise of the present analysis depends on what happens in the immediate vicinity of the breakdown region, we shall augment the more conventional approximation with a term taking proper account of the time dependent term of Hamiltonian (4) in the average dynamics.

We thus proceed to the derivation of our ponderomotive approximation.

III. A CANONICAL TRANSFORMATION LEADING TO THE PONDEROMOTIVE APPROXIMATION

Our ponderomotive approach basically tries to seek a canonical transformation with which one can consistently remove all high-frequency terms in the governing Hamiltonian. The procedure, if successful, converts all dynamical variables into their average form as mentioned above [19–21]. To perform the canonical transformation we start from the exact Hamiltonian (4) and make use of a generating function of the form $F = F(x, P_x, t) = xP_x + f(x, P_x, t)$ [22]. Accordingly, the relevant variables transform as

$$p_x = P_x + \partial f/\partial x, \tag{5}$$

$$X = x + \partial f/\partial P_x, \tag{6}$$

and

$$\mathcal{H} = H + \partial f/\partial t, \tag{7}$$

where $X, P_x, \mathcal{H}$ are the transformed variables. The function f must be such that the new Hamiltonian $\mathcal{H}$ and new variables X and P_x are free of high-frequency terms.

The Hamiltonian H contains both time dependent and time independent terms, the former emerging from the beat-wave term. The ponderomotive approximation we seek should be able to single out the average effect of this time dependent term on the average particle dynamics.

One can expect the ponderomotive approach to become a little intricate in the present case, in virtue of the square root character of the original Hamiltonian (4). Since we do not wish to compromise the validity of the approach at high-intensity fields, we shall attempt to write the ponderomotive Hamiltonian in the form

$$\mathcal{H} = \sqrt{1 + P_x^2/\alpha + A_{l,0}^2 + A_{w,0}^2 e^{-\frac{X^2}{\sigma^2}} + h(X, P_x)}, \tag{8}$$

where the as yet unknown term $h(X, P_x)$ incorporates the average effect of the high-frequency beat term involving the product of the arbitrary amplitudes A_{w0} and A_{l0}. The function h is not assumed small, appearing at the same magnitude level as both amplitudes, and this is why we include h in the radicand and not somewhere else.

If one demands that the generating function f be free of secularly growing terms then h can be calculated. The first step towards its evaluation is simply to use equations (5), (7) and (8) to obtain

$$\sqrt{1 + (P_x + \partial f/\partial x)^2/\alpha + A_{l,0}^2 + A_{w,0}^2 e^{-\frac{x^2}{\sigma^2}} + 2A_{l,0}A_{w,0}e^{-\frac{x^2}{2\sigma^2}}\cos(x-t)} + \frac{\partial f}{\partial t} = \sqrt{1 + P_x^2/\alpha + A_{l,0}^2 + A_{w,0}^2 e^{-\frac{x^2}{\sigma^2}} + h(x, P_x)}. \tag{9}$$

One then transposes the $\partial f/\partial t$ term to the right-hand-side, squares both sides of the resulting expression, and ends up with a closed equation for f:

$$2\mathcal{H}\frac{\partial f}{\partial t} + \frac{2P_x}{\alpha}\frac{\partial f}{\partial x} = \left(\frac{\partial f}{\partial t}\right)^2 - \frac{1}{\alpha}\left(\frac{\partial f}{\partial x}\right)^2 - 2A_{l,0}A_{w,0}e^{-\frac{x^2}{2\sigma^2}}\cos(x-t) + h(x, P_x). \tag{10}$$

This is a non-linear equation for the high-frequency variable f, which therefore requires the condition

$$h = -\left\langle \left(\frac{\partial f}{\partial t}\right)^2 - \frac{1}{\alpha}\left(\frac{\partial f}{\partial x}\right)^2 \right\rangle_\theta \tag{11}$$

- the symbol $\langle\rangle_\theta$ indicating average over fast variables - in order to cancel out the average driving terms present on its right-hand-side. We solve the pair of equations (10) and (11) by means of a harmonic expansion for f. More to the point, we write $f = f_1(\theta) + f_2(2\theta) + ...$ with $\theta = x - t$ and $\langle f_n\rangle_\theta = 0$, neglect in this first approach higher harmonics than the second, but do not necessarily assume f_1 small. The critical assumption here is that higher-harmonics make a small correction to the full form of function f, which is something that shall be verified when the time comes to compare theory and numerics.

Under these conditions,

$$f_1 = \frac{1}{\mathcal{H}}\frac{1}{\left(1-\frac{P_x}{\alpha\mathcal{H}}\right)}A_{l,0}A_{w,0}e^{-\frac{x^2}{2\sigma^2}}\sin(x-t), \qquad (12)$$

allowing us to obtain an approximate expression for h in the form

$$h = -\frac{1}{2}\left(1-\frac{1}{\alpha}\right)\frac{A_w^2A_l^2e^{-\frac{x^2}{\sigma^2}}}{(P_x/\alpha-\mathcal{H})^2}. \qquad (13)$$

Expression (13) is still a difficult one to solve, the reason being the presence of h in the factor $\mathcal{H}$ (see Eq. (8)) on its right-hand side. A full solution can be actually obtained for relation (13), but in order to have a manageable one we approximate h in $\mathcal{H}$ by the value it would take had we truncated the theory to first harmonic terms. In this case the condition for the absence of secular terms would be $h = 0$ which we therefore take as our initial approximation allowing us to obtain an improved value from relation (13).

Putting together expressions (8) and (13) and replacing x with X in the very slowly modulated amplitudes where the replacement is allowable ($(x-X)/\sigma \ll 1$), one finally arrives at the ponderomotive Hamiltonian,

$$\mathcal{H} = \sqrt{1 + P_x^2/\alpha + A_{l,0}^2 + A_{w,0}^2e^{-\frac{X^2}{\sigma^2}} - \frac{1}{2}\left(1-\frac{1}{\alpha}\right)\frac{A_w^2A_l^2e^{-\frac{X^2}{\sigma^2}}}{(P_x/\alpha-\Gamma)^2}} \qquad (14)$$

($\Gamma \equiv \sqrt{1 + P_x^2/\alpha + A_{l,0}^2 + A_{w,0}^2e^{-\frac{X^2}{\sigma^2}}}$), whose dynamics shall later be compared with that provided by the exact Hamiltonian (4).

As mentioned earlier, the full ponderomotive Hamiltonian (14) inherits an explicit contribution from the wave-particle resonances that are potentially present in the physics of the problem, as described by the exact form (4). This contribution is represented by the last term within the square root of expression (14), which becomes increasingly relevant as one approaches resonance. Away from resonance, where this term could arguably be dropped, one would obtain the more conventional form of the ponderomotive approximation where only quadratic forms involving the slowly modulated laser's and wiggler's individual amplitudes are present [13].

IV. RESONANT TRAPPING

As discussed in the Introduction, the idea of this work is to drive particles with the ponderomotive forces up to a point where trapping in the potential troughs of the high-frequency beat-wave takes place. Under this circumstance, where the ponderomotive approximation is no longer valid, the focus of interest turns to how much energy particles can gain from the resonant process. With the help of relativistic electrostatic models, it has been shown that the gain may be considerable [7, 15, 23] and the purpose of this section is to investigate the case where the inverse FEL-like configuration replaces the electrostatic model.

Estimates are developed along the lines of previous work [7]. In other words, we make use of the fact that on the verge of trapping, particles that were initially lagging the beat-wave have been accelerated by the ponderomotive field and are now moving with nearly the beat-wave's phase velocity. We use this configuration as an initial condition to calculate the maximum velocity, disregarding the slow laser modulation in this fast and short-length trapping and acceleration process.

Since we discard slow modulation in the trapping process, the dynamical system becomes one degree of freedom (it now depends only on the single phase $\theta = x - t$) and a constant of motion can be obtained in the form

$$H - p_x = Constant. \qquad (15)$$

Recalling that $v_x = \partial H/\partial p_x$ we can rewrite expression (15) entirely in terms of the particle speed, and imposing the initial condition that $v_x = 1$ at $\theta\ (mod\ 2\pi) = 0$, one can obtain the maximum velocity at $\theta\ (mod\ 2\pi) = \pi$ in terms of the laser and wiggler amplitudes A_{l0} and A_{w0} for any given α. Note that we will always pick the positive root of relation (15) at $\theta = \pi$. The positive root is accompanied by a negative root whose modulus is,

however, always smaller due to the positive propagation direction of the trapping carrier.

A simple expression for the maximum velocity, valid when the dimensionless laser and wiggler amplitudes (also referred to as the wiggler strength parameter) are much larger than the unity, takes the following form

$$\frac{v_{x,dim}(\theta=\pi)}{c} = v_x\sqrt{\alpha} \underset{A_{w0},A_{l0}\gg 1}{\longrightarrow} \frac{\sqrt{\alpha}(f-1)^2+2\sqrt{(\alpha-1)^2f(f+1)^2}}{f(-4\alpha+f+2)+1} + \mathcal{O}(\frac{1}{A^2_{(l,w)0}}) \sim \begin{cases} \sqrt{\alpha} & \text{if } 0<f\ll 1 \text{ or } f\gg 1 \\ 1 & \text{if } f\to 1, \end{cases} \tag{16}$$

where the fraction f is introduced as $f = A_{l0}/A_{w0}$. The truly remarkable aspect suggested by approximation (16) is that acceleration is optimal and unimpeded when laser and wiggler have the same amplitude: the larger the common amplitude fields are, the closer to c the maximal velocity is. On the other hand, if $f \neq 1$, there will be a limit for the maximum velocity at some point between the phase-velocity of the beat mode $c\sqrt{\alpha}$ and the speed of light, no matter how large the fields are. The maximum velocity of the particle does not significantly depend on its initial phase.

To have a general view of the acceleration efficiency we introduce the velocity gain $G_{v_\pi} \equiv Log[(1-\sqrt{\alpha})/(1-\sqrt{\alpha}v_x(\theta=\pi))]$ measuring how close to c is the maximum velocity in comparison with the phase velocity. Then we produce the color graded plot of Fig. 1 to represent G_{v_π} in terms of the normalized laser and wiggler amplitudes. The figure indeed shows that unless one works with equal amplitude waves, acceleration is not optimal. Even if one increases both amplitudes, keeping the two of them unequal with $f \neq 1$ limits the maximum velocity. On the other hand, when $f = 1$ the maximum, velocity can be as close to c as one wishes, all depending on the choice of the proper common mode amplitudes, whose extended range seen in the figure is compatible with the intensities generated in current petawatt and future exawatt high-frequency lasers [24] and self-focused infrared lasers of relativistically high intensities [25].

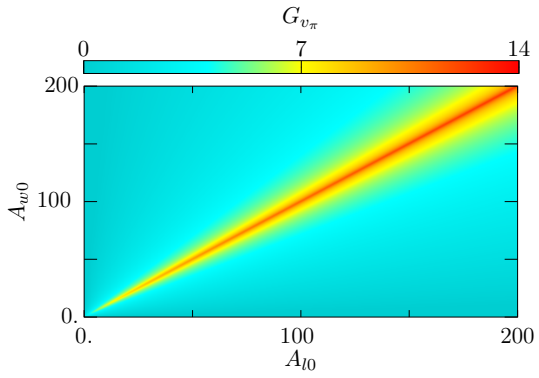

FIG. 1: Color graded map for G_{v_π} in terms of laser and wiggler amplitudes. We take $\alpha = 0.9$.

V. NUMERICAL ANALYSIS OF PONDEROMOTIVE, RESONANT AND ACCELERATING REGIMES

We now perform the exact numerical analysis of the dynamics, identifying the ponderomotive and trapping regimes and comparing numerical results with the respective analytical results. As mentioned in the Introduction, special attention will be given to the breakdown of the ponderomotive regimes, where resonant trapping and efficient acceleration are expected to occur. The analysis will be conducted as the injection velocity v_0 is varied. We consider $\alpha = 0.9$, $\sigma = 10^3$, $A_{w0} = A_{l0} = 10^2$, and $x(t=0) = -10\,\sigma$, unless otherwise stated. We point out that as far as the width σ is much larger than the wiggler wavelength, its exact extension does not affect the outcome of the acceleration process. We verified that $\sigma = 100$ is still fine, but that shorter widths does affect the efficiency of the adiabatic process leading to acceleration.

A. The ponderomotive regime

In panel (a) of Fig. 2 we start the analysis by offering a view on the exact dynamics as obtained from the full Hamiltonian (4). The injection velocity seen in the plot is low enough that trapping is absent, so the entire dynamics remains in the ponderomotive regime. Two curves representing the particle velocity are drawn: the blue one depicts the raw solution for the Hamiltonian dynamics, and the red represents the average of this raw solution taken over narrow temporal-windows, each window involving a large number of high-frequency oscillations. We indeed see that the particle velocity always remains below the dashed light brown line representing the phase-velocity $\sqrt{\alpha}$ of the high-frequency driver mode.

From both curves one observes the typical double hump dynamical profile, as particles travel across the localized field whose peak sits right at the central depression. The average velocity is always positive, so in this case one is observing passing particles.

The double hump, the characteristic signature under the condition of nearly resonant particles driven by equal and large amplitude fields, means that as particles are injected in the modulated carrier, they go through stages of

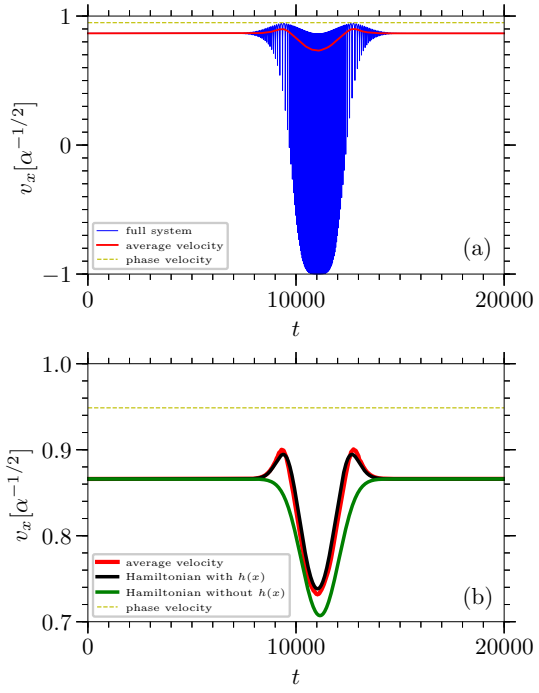

FIG. 2: Velocity versus time for passing particles with injection velocity $v_0\sqrt{\alpha} = v_{0,dim}/c = 0.867$. In panel (a) we plot the full solution from the exact Hamiltonian (4) and the respective time average curve. In panel (b) the time average curve of the exact solution is compared with the solution of the ponderomotive Hamiltonian (14), with and without the h-term correction (see Eqs. (8) and (14)) .

uphill acceleration. This is a rather unexpected feature, as the most usual sort of acceleration in ponderomotive regimes is the downhill one, where particles are pushed back, and not attracted by the potential.

Uphill acceleration has been studied in some cases with help of Lagrangian approaches [12, 15]. The Lagrangian approach provides valuable information, being however entirely consistent only when the average velocity bears a monotonic relationship with the modulated potential. This latter fact is observed by the use of the energy conserving form $E = v\partial L/\partial v - L$, which produces a relation between any given velocity and the field intensity present in L [14]. This is not what happens here since either to the right-hand side or left-hand side of the symmetric central depression, particles cross points of different field intensities with the same velocity.

We then proceed to Fig. 2 (b) where the average of the fully numeric solution (red) for the particle velocity is compared with the average velocity as obtained from the canonically derived ponderomotive Hamiltonian (5), both with the h-corrective term turned on (black) and off (green). The figure shows that the presence of the h term in the ponderomotive Hamiltonian perfectly adjusts the resultant dynamics to the fully numerical curve. On the other hand, as one takes $h \to 0$ the resulting curve is purely downhill (particles are repelled from the potential) as found in the Lagrangian theories.

To emphasize the role of the h-term we also consider the case of smaller injection velocities. Keeping the same field amplitudes, one would expect particles to be reflected by the localized beat mode under these circumstances. This is what the final negative velocity of Fig. 3 indeed reveals, albeit with some distinguishable effects due to uphill acceleration present once again. In the figure, where α is also lowered in order to enhance the approach to resonant effects ($\alpha = 0.77$), one again observes particle being initially *attracted* by the localized field (notice the upward distortion in the incoming orbital leg) only to be ultimately reflected later on, with the final negative velocity. Comparisons with h turned on and off are again displayed with the present model showing good agreement with full simulations, including the region where particle velocities are reversing.

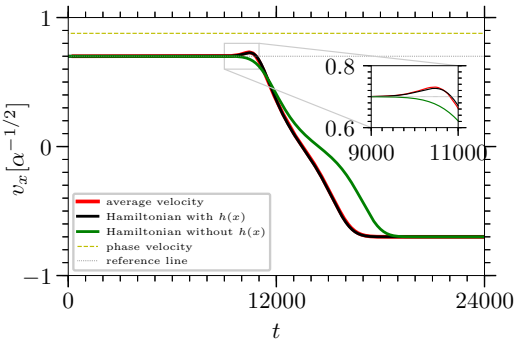

FIG. 3: Velocity versus time for reflected particles, displaying comparisons of the time averaged exact solution, and the ponderomotive solution with and without the h term present. In the present case we consider $\alpha = 0.77$.

The importance of correctly describing the peaks of the double hump profile seen in panel (a) of Fig. 2 or the single hump of Fig. 3, is that these peaks are in fact the first segments of a particle orbit to be captured by the carrier mode as the injection velocity grows. Let us see next how the orbit evolves when this resonant trapping takes place.

B. Breakdown of the pondermotive regime, trapping and resonant acceleration

We focus on the case of panel (a) of Fig. 2; the relevant points of the pertinent discussion are equivalent for the case of reflected particles represented in Fig. 3.

If one takes the injection velocity a little higher than the one seen in in Fig. 2 (a), particles are captured at the earliest (leftmost) velocity peak. According to the case $f = 1$ of expression (16), velocities jump to some point close to the speed of light when the amplitudes are large and this is what can be observed from Fig. 4.

The acceleration process here differs from what has been previously seen in the context of electrostatic

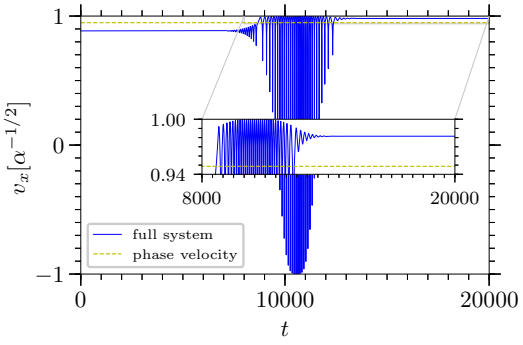

FIG. 4: Extreme acceleration as particles are captured by the resonance beat mode. The inset reveals how close to the speed of light the particle can reach after capture; the numerical maximum of the velocity yields 1-$\sqrt{\alpha}v_{x_{max}} \sim 10^{-6}$, with $\alpha = 0.9$, $v_0\sqrt{\alpha} = v_{0,dim}/c = 0.87$.

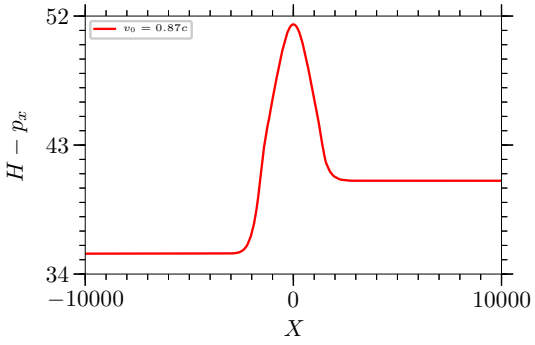

FIG. 5: Adiabatic variations of $H - p_x$ indicating reversibility at $X = 0$ but not at the left/right ends of the plot.

modes, where particles are catapulted at a single field maximum then continue with a velocity above the phase velocity. Here particles are trapped at the leftmost peak of Fig. 2 where the modulated field has not yet reached its maximum located at $x = 0$. Therefore particles cannot overtake the next, higher potential crest, and remain oscillating in the wave trough for a long period of time while undergoing a slow adiabatic energy exchange process along the way [7, 23]. The adiabatic gain reaches its peak at the maximum of the modulated field envelope and shortly after the energy exchange reverses as the fields start to decrease. As a result particles eventually leave the field region with lower velocities than the maximum, a fact that suggests that it would be useful to perform extraction near the envelope peak. The final velocity of the particle depends on its initial phase, while the maximum velocity does not.

An excellent variable one can use to follow the adiabatic process is provided by the combination $H - p_x$ introduced by Eq. (4) The variable is rigorously constant in the case of spatially uniform fields and is expected to display slow adiabatic variations in the presence of slow spatial modulations.

This is almost precisely what Fig. 5 shows, but not quite. Due to the trapping/detrapping events on both sides of the potential hump, the evolution of $H - p_x$ is not reversible at all times: the injection velocity, which incidentally barely crosses the trapping threshold, may differ from the final velocity v_f as the particle breaks away from the localized pulse. However, the dynamics is smoothly adiabatic along its way to X=0 which reiterates the fact that this is the ideal locus for particle extraction.

The adiabatic process traps and efficiently accelerates the electron in the resonance. In a way, the traditional tapering is here replaced by the slow change of the wiggler amplitude.

We also created Fig. 6 in order to examine how the acceleration process responds to increasing amplitudes of the electromagnetic fields. The figure displays once again the velocity gain, but this time for the full modulated problem and not simply the constant amplitude idealised model analysed in Fig. 1 . The injection velocity is such that the particle orbit is barely touching the resonant line and therefore just getting trapped in the beat driver. We measure the gain as $G_{v_{max}} = Log[(1-\sqrt{\alpha})/(1-\sqrt{\alpha}(v_x)_{max})]$ where $(v_x)_{max}$ is the absolute maximum velocity the particle reaches, and observe that it follows closely its counterpart as defined in Fig. 1. It appears that even though in the modulated case trapping occurs at lower field amplitudes, once the adiabatic process takes over it follows the oscillatory dynamics approximately to the same maximal velocity as in the uniform case.

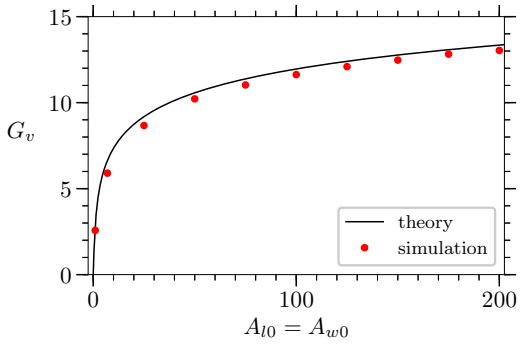

FIG. 6: Maximum gain of the fully modulated case (red dots) compared with the theoretical gain of the uniform amplitude case as in Fig. 1. Once again, $\alpha = 0.9$.

In a very low density limit, the beam can be thought as a collection of single particles, in a way the interaction among them can be neglected of their dynamics. The maximum velocity of the particle, as in many accelerator devices, depends on its initial phase. In order to analyse the behaviour of the velocities at the moment a particle reaches its maximum velocity, we introduce a new parameter in the system: the initial phase, θ_0. This phase can be simply added to the definition of θ_l, resulting in $\theta_l = k_l x - \omega_l t + \theta_0$. The initial phase emulates the initial conditions of the beginning of the particle dynamics.

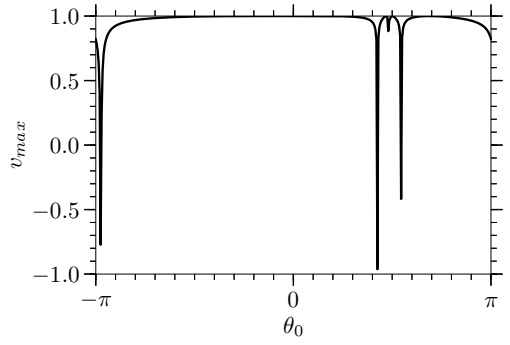

FIG. 7: Velocity of the particles as a function of the initial phase, θ_0 of the particle at the moment where the velocity is maximum for $\theta_0 = 0$. Parameters are the same as in Fig. 4.

In the present model, as can be seen in Fig. 7, there are very narrow regions of θ_0 where the velocity of the particle at the moment the particle initially located at $\theta_0 = 0$ reaches its maximum velocity is lower than the phase velocity. The narrow regions are interleaved with plateaux of near-c velocities. This is a desirable feature for accelerators.

The length of the particle bunch, for a very low density limit, to obtain consistent acceleration (which is directly related to the phase-acceptance) is, for the parameters used in Fig. 7, in the order of the half length of the ponderomotive potential, which in turn is equal to $\lambda_p = 2\pi/k_p$, with $k_p = k_w + k_l$ (from $\theta_0 \approx -\pi$ to $\theta_0 \approx \pi/2$). In the cases where $k_l \gg k_l$, the bunch length is $\approx \lambda_l/2$, where $\lambda_l = 2\pi/k_l$.

If the final velocities of the particles were plotted in Fig. 7, the plateaux should be even more pronounced, while the negative velocities should not be present.

C. General view of the dynamical regimes

At this point one is aware that the model investigated here has three operational regimes: (i) a ponderomotive regime of passing particles - where particles sweep across the localized field without trapping and any energy gain, (ii) a ponderomotive regime of reflected particles - where particles are reflected back off the localized field, again with no trapping and no net energy gain and (iii) a trapping regime where ponderomotive approximations break down and particles are captured by the wave troughs of the beat-wave field with subsequent large amounts of energy gain.

One can visualise all regimes and the respective transitions from one to another with color graded maps for the final (exiting) forward or backward velocity v_f.

In Figs. 8 (a) and (b) we represent the final velocity in terms of the common field amplitude and the injection velocity for the two values of α used in the analysis of subsection V A. As already suggested by the analysis of Figs. 2 and 3 where the transition from ponderomotive regimes

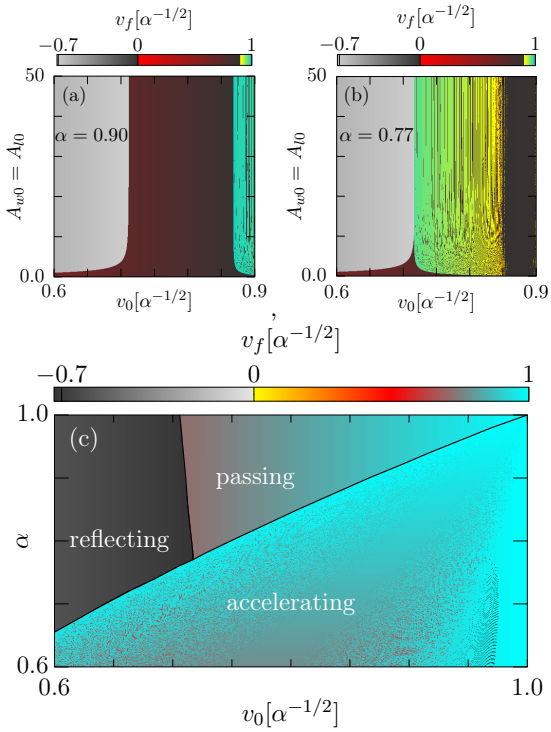

FIG. 8: Color graded maps for the final velocity, with independent variables indicated in the axes of the plots. In panel (c) we take both waves with equal normalized amplitudes $A_{w0} = A_{l0} = 25$.

to trapping is imminent, one sees from the present Fig. 8 (a) that while for the larger value of $\alpha\,(= 0.9)$ trapping is preceded by a ponderomotive regime of passing particles, for the smaller $\alpha\,(= 0.77)$ of panel (b), trapping is mostly preceded by the reflective ponderomotive regime where the final velocities are negative. We point out the presence of less-than-effective discrete curves inside the accelerating regions in Figs. 8 (a) and (b). The position of these curves depends on the initial phase of the particle. Although the maximum velocity of the particle does not depend on its initial phase, the final velocity does.

For a given value of the common field amplitude, there is thus an important structural change in the trapping patterns and subsequent resonant acceleration as the phase velocity of the driver mode changes. We attempt to represent this change in our last Fig. 8 (c), where the color graded map for the final velocity is depicted in terms of the injection velocity and of the phase-velocity α for a given mode amplitude, which is chosen to be $A_{w0} = A_{l0} = 25$ here. One indeed notes that while for small α's there is direct transition from reflection to trapping, for α's larger than a critical value that lies around $\alpha = 0.78$, the reflective regime first turns into a passing regime and only then, for larger values of the injection velocity, trapping takes place.

Finally we extend the discussion on the model parameters in a very brief way. First, the wiggler must be intense. Considering a magnetic

field generated by super-conducting coils, one can achieve magnetic fields B_w of magnitudes up to 10 Tesla.

If one then takes a wiggler spacing of $\lambda_w \sim 10$ cm, a wiggler strength parameter of magnitude $A_w \sim 100$ is obtained. With $\lambda_w \sim 10$ cm, considering the dimensionless phase-velocity $v_{phase}/c \equiv \sqrt{\alpha} = 1/(1 + k_w/k_l)$ with $k_{l,w} \sim 1/\lambda_{l,w}$, and taking α around 0.9 as discussed here, one would obtain $\lambda_l \sim 5$ mm. This sits at the upper-wavelength edge of the far-infrared laser spectrum. Increasingly larger values of α's would select shorter and shorter laser wavelengths, which would be likewise describable by the present formalism.

With $\sigma \sim 1000$ along with the obtained wavevectors, after reverting to dimensional variables we estimate that a laser path and wave-particle interaction length of the order of 5 meters would suffice for full and efficient interaction. Under these conditions of a long path with relatively large laser wavelengths, constraints due to diffraction and spot sizes are relatively unimportant. A summary can be seen in table I.

TABLE I: Summary of Parameters

α	0.9
B_w	~ 10 Tesla
λ_w	10 cm
λ_l	~ 5 mm
Length	~ 5 m

VI. CONCLUSION

As mentioned in the Introduction, this paper has been dedicated to extending ideas developed in a previous paper, where efficient particle acceleration has been obtained at the transitional phase between ponderomotive and resonant regimes provided by slowly modulated plasma waves. Here we replace the plasma waves with an inverse free-electron laser scheme, in an attempt to obtain the same accelerating efficiency through a more stable system than the one usually associated with waves in plasmas.

We have shown that acceleration is indeed equally efficient here. By means of a ponderomotive approximation based on a canonical Hamiltonian formalism that reproduces key elements of the particle dynamics near the wave-particle resonance, accurate results are obtained. This accuracy cannot be obtained with the usual cycle average of the Lagrangian approach. Analysis of these results indicates that the ponderomotive force pulls particles toward resonance, and that once trapped by the resonances acceleration towards the speed of light is unimpeded if laser and wiggler both have the same amplitude.

In a slight variation with respect to the case of plasma waves, here particles are captured by the resonance before the peak of the slowly varying envelope of the high-frequency carrier. As observed earlier, under these conditions particles cannot be slung forward across the entire potential hump because the wave crest ahead of the particle is slightly larger than the one behind. Particles are therefore trapped in the resonant trough and energy gain follows an adiabatic path towards the peak of the modulated drive where gain is maximum. Shortly after the peak the adiabatic process reverses and particles start to lose energy, so one should find a way to extract particles at the envelope maximum.

One possible way to optimize extraction would be to truncate the wiggler operation only up to $x = 0$. If the wiggler is limited this way, particles in principle would be ejected forward at $x = 0$ with no further energy loss. This application is under current study and more conclusive results shall be reported.

Self-consistent effects due to the wave and particle interaction were not considered in the present analysis. Nonlinear wave-particle self-consistent dynamics involving large wave amplitudes and very dense particle populations might affect diffraction, refraction and proper tuning between particles and the resonant velocity formed by laser and wiggler. Self-consistency under these conditions may be relevant and should be analysed in future investigations.

Acknowledgments:

We acknowledge support from CNPq and CAPES, Brasil, and from AFOSR, USA, under research grant FA9550-16-1-0280. S.M. acknowledges support from Grant No. ANR-11-IDEX-0004-02 Plas@Par. R.A.C. is supported by the UK Science and Engineering Research Council grant EP/N028694/1. **We also thank important remarks and suggestions by the anonymous reviewers.**

[1] R. Z. Sagdeev and V. D. Shapiro, Pis'ma Zh. Eksp. Teor. Fiz. **17**, 389 (1973) [JETP Lett. **17**, 279 (1973)].

[2] T. Tajima and J. M. Dawson, Phys. Rev. Lett. **43**, 267 (1979).

[3] T. Katsouleas and J. M. Dawson, Phys. Rev. Lett. **51**, 392 (1983).

[4] P. K. Shukla, N. N. Rao, M. Y. Yu, and N. L. Tsintsadze, Phys. Letts. **138**, 1 (1986).

[5] R. Bingham, Nature **424**, 258 (2003).

[6] M. Tzoufras, W. Lu, F. S. Tsung, C. Huang, W. B. Mori, T. Katsouleas, J. Vieira, R. A. Fonseca, and L. O. Silva, Phys. Rev. Lett. **101**, 145002 (2008).

[7] S. Marini, E. A. Peter, G. I. de Oliveira, and F. B. Rizzato, Phys. Plasmas **24**, 093113 (2017).

[8] J. T. Mendonça, *Theory of Photon Acceleration.* IOP Publishing, Bristol (2001).

[9] L. F. Monteiro, A. Serbeto, K. H. Tsui, J. T. Mendonça, and R. M. O. Galvão, Phys. Plasmas **20**, 073101 (2013).

[10] E. Peter, A. Endler, and F. B. Rizzato, and A. Serbeto, Phys. Plasmas **20**, 123104 (2013).

[11] E. Peter, A. Endler, and F. B. Rizzato, J. Plasma Phys. **83**, 905830302, (2017).

[12] P. Mulser and D. Bauer, *High-Power Laser-Matter Interaction*, Springer-Verlag, Berlin (2010).

[13] A. Macchi, *A Superintense Laser-Plasma Interaction Theory Primer*, Springer, London (2013).

[14] D. A. Burton, R. A. Cairns, B. Ersfeld, A. Noble, S. Yoffe, and D. A. Jaroszynski, *Observations on the ponderomotive force*, Proc. SPIE **10234**, *Relativistic Plasma Waves and Particle Beams as Coherent and Incoherent Radiation Sources II*, 102340G doi:10.1117/12.2270542 (2017).

[15] I. Almansa, D. Burton, R. A. Cairns, S. Marini, E. Peter, F. B. Rizzato, and F. Russman, Phys. Plasmas, **25**, 113107 (2018).

[16] M. Raynaud, J. Kupersztych, C. Riconda, J. C. Adam, and A. Heron, Phys. Plasmas **14**, 092702 (2007).

[17] J. P. Blewett and R. Chasman, J. App. Phys. **48**, 2692 (1977).

[18] E. G. Evstatiev, P. J. Morrison, and W. Horton, Phys. Plasmas **12**, 072108 (2005)

[19] J. R, Cary J R and A. N. Kaufman, Phys. Fluids **24**, 1238 (1981).

[20] C. Grebogi and R. G. Littlejohn, Phys. Fluids **27**, 1996 (1984).

[21] D. E. Ruiz and I. Y. Dodin, Phys. Rev. A **95**, 168 (2017).

[22] H. Goldstein, *Classical Mechanics*, Addison-Wesley (Second Edition), Reading, Massachusetts (1980).

[23] F. B. Russman, S. Marini, E. A. Peter, G. I. de Oliveira, and F. B. Rizzato, Phys. Plasmas **25**, 023110 (2018).

[24] A. Sharma, Scientific Reports **8**, 2191 (2018).

[25] X. Yang, E. Brunetti, and D. Jaroszynski, New J. Phys. **20**, 043046 (2018).

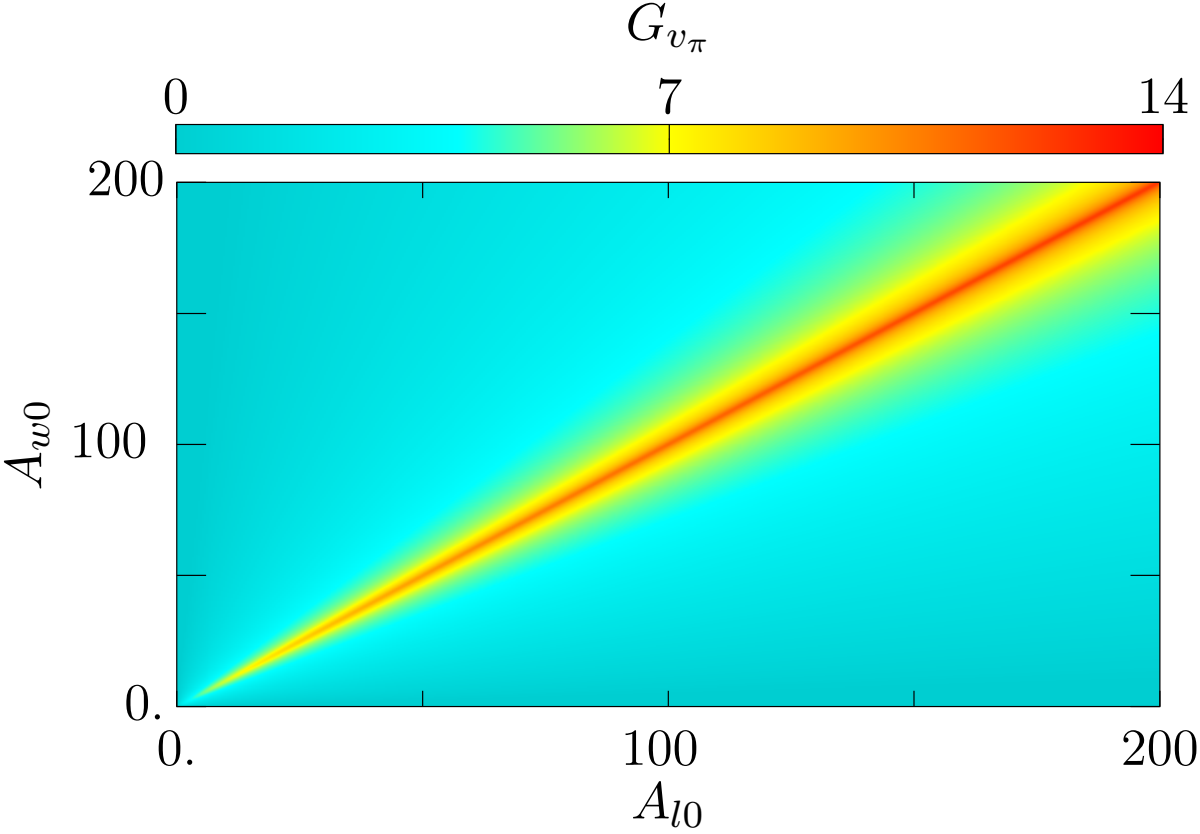
G_{v_π}
0
7
14
200
100
0.
A_{w0}
0.
100
200
A_{l0}

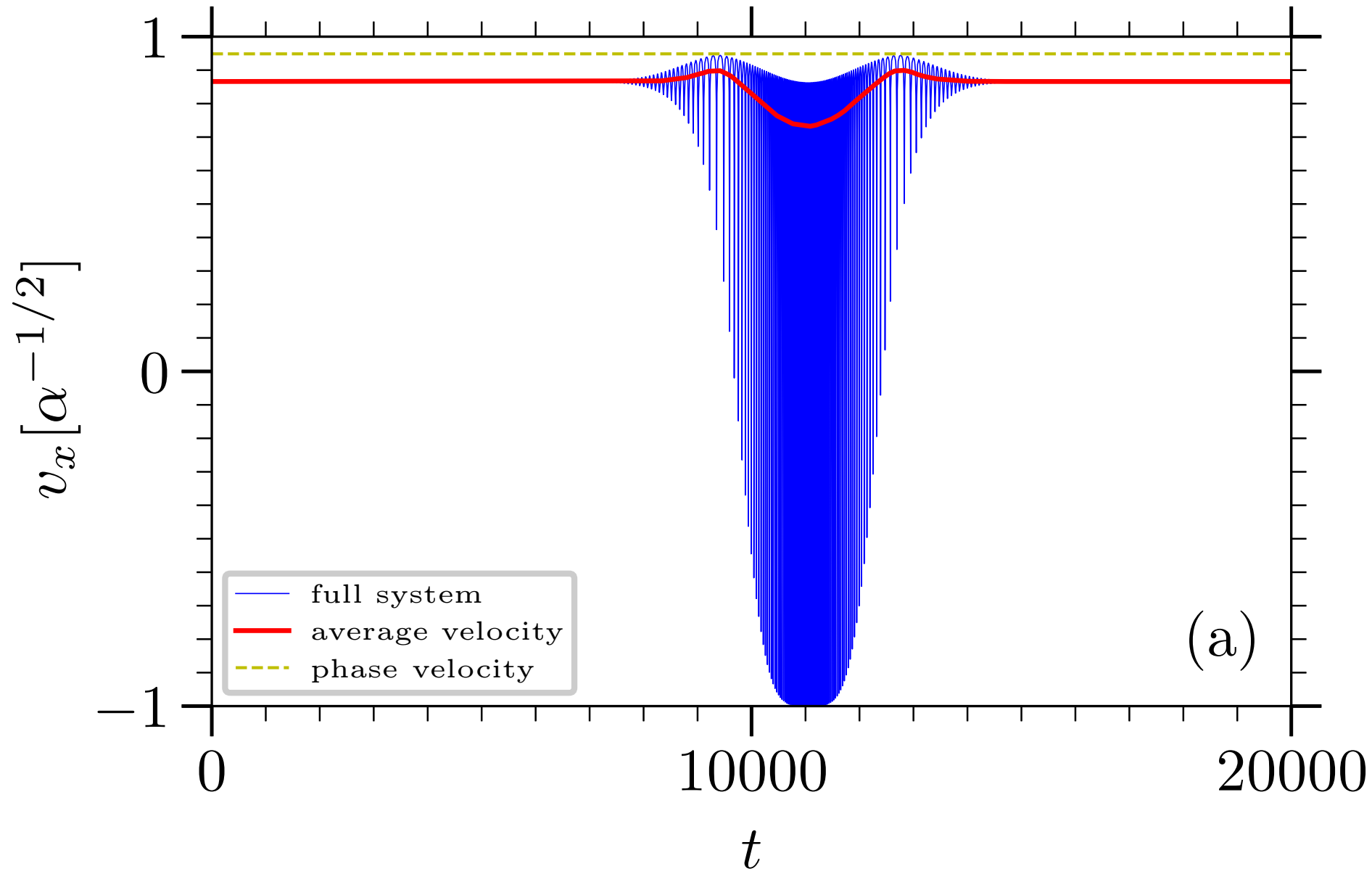
1
0
−1
0
10000
20000
$v_x\,[\alpha^{-1/2}]$
t
full system
average velocity
phase velocity
(a)

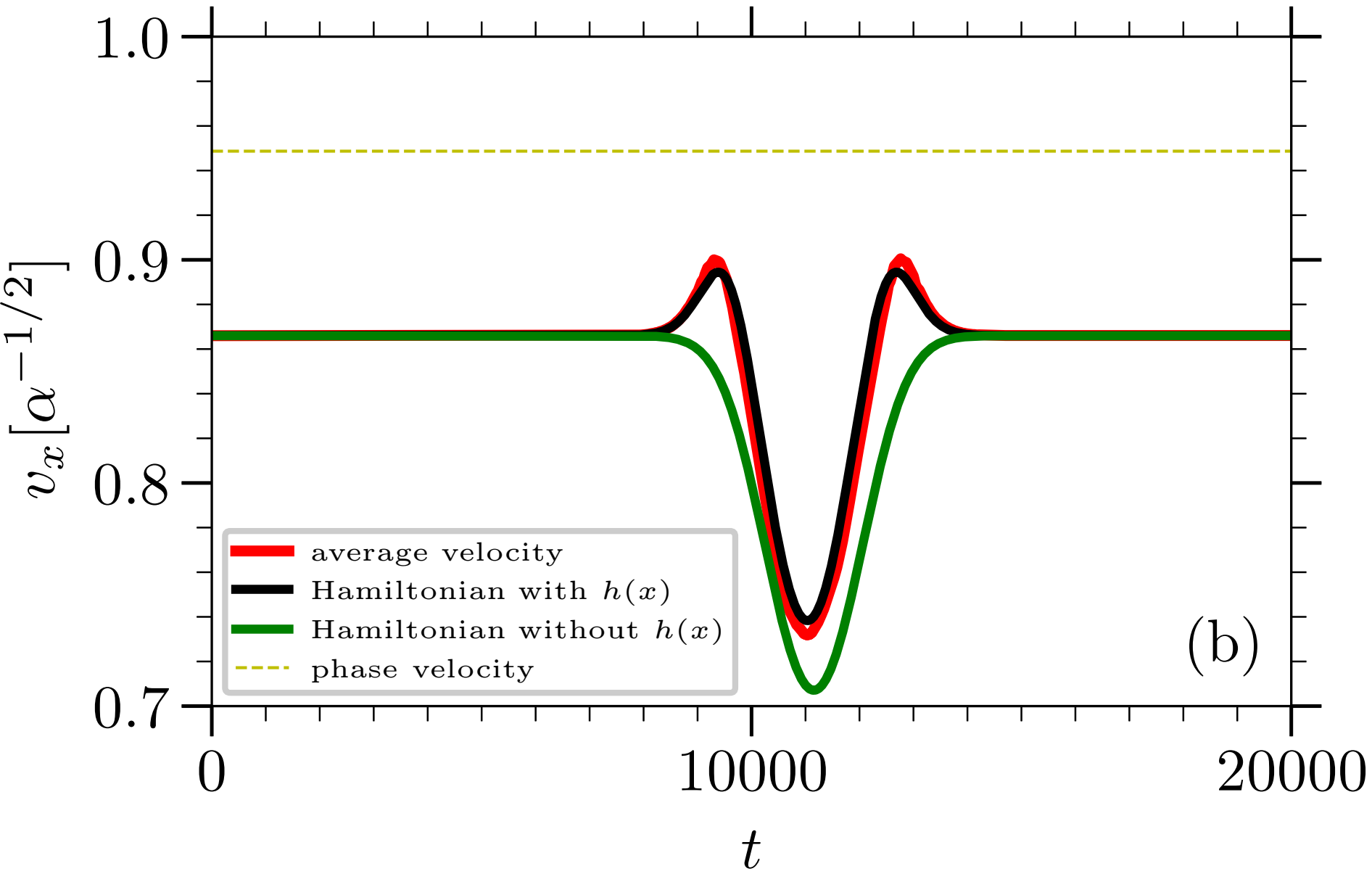
1.0
0.9
0.8
0.7
$v_x\,[\alpha^{-1/2}]$
0
10000
20000
t
average velocity
Hamiltonian with $h(x)$
Hamiltonian without $h(x)$
phase velocity
(b)

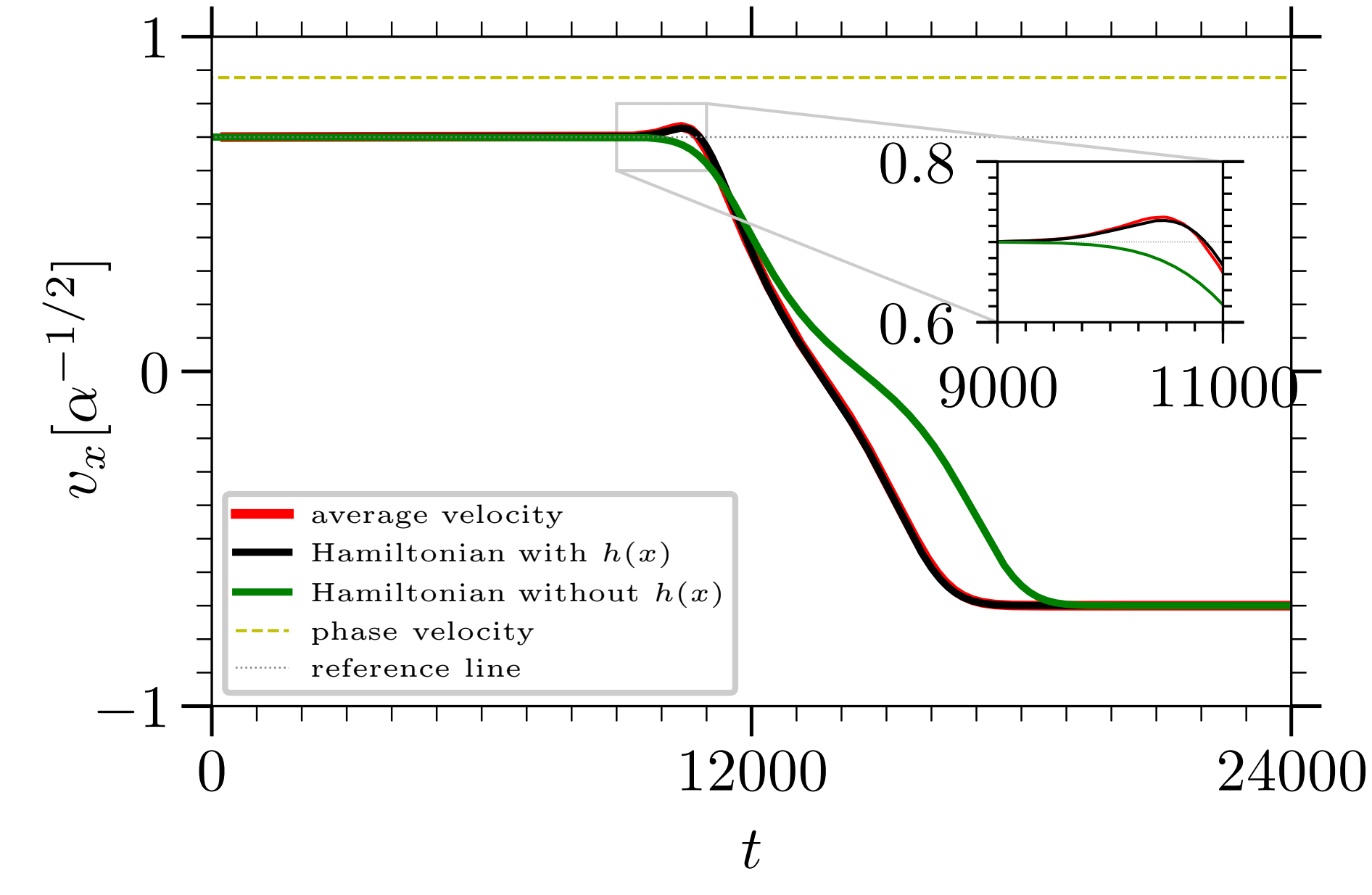
1
0
−1
$v_x\,[\alpha^{-1/2}]$
0
12000
24000
t
0.8
0.6
9000
11000
average velocity
Hamiltonian with $h(x)$
Hamiltonian without $h(x)$
phase velocity
reference line

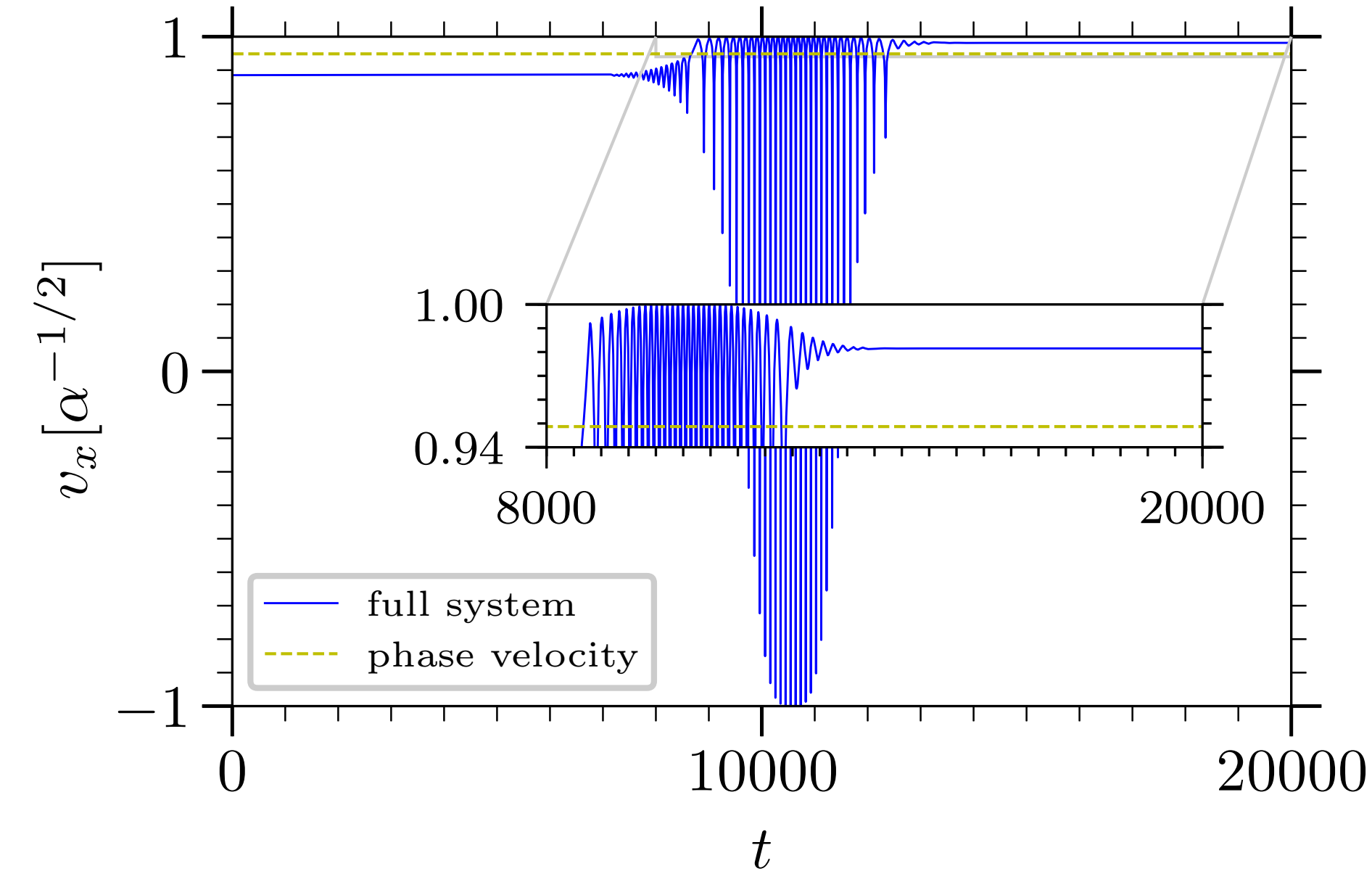
1
0
−1
$v_x\,[\alpha^{-1/2}]$
0
10000
20000
t
1.00
0.94
8000
20000
full system
phase velocity

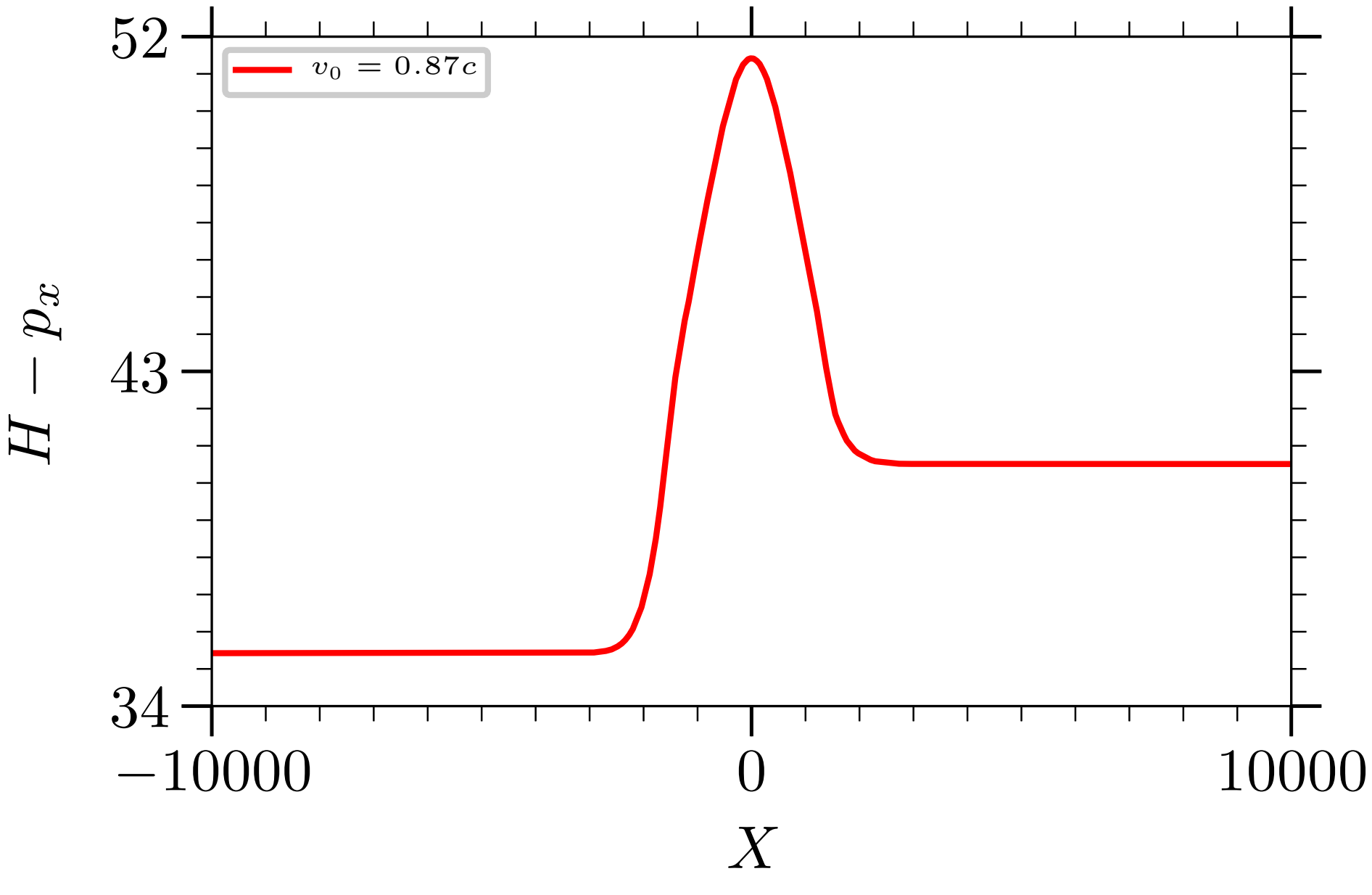
$v_0 = 0.87c$
52
43
34
$H - p_x$
−10000
0
10000
X

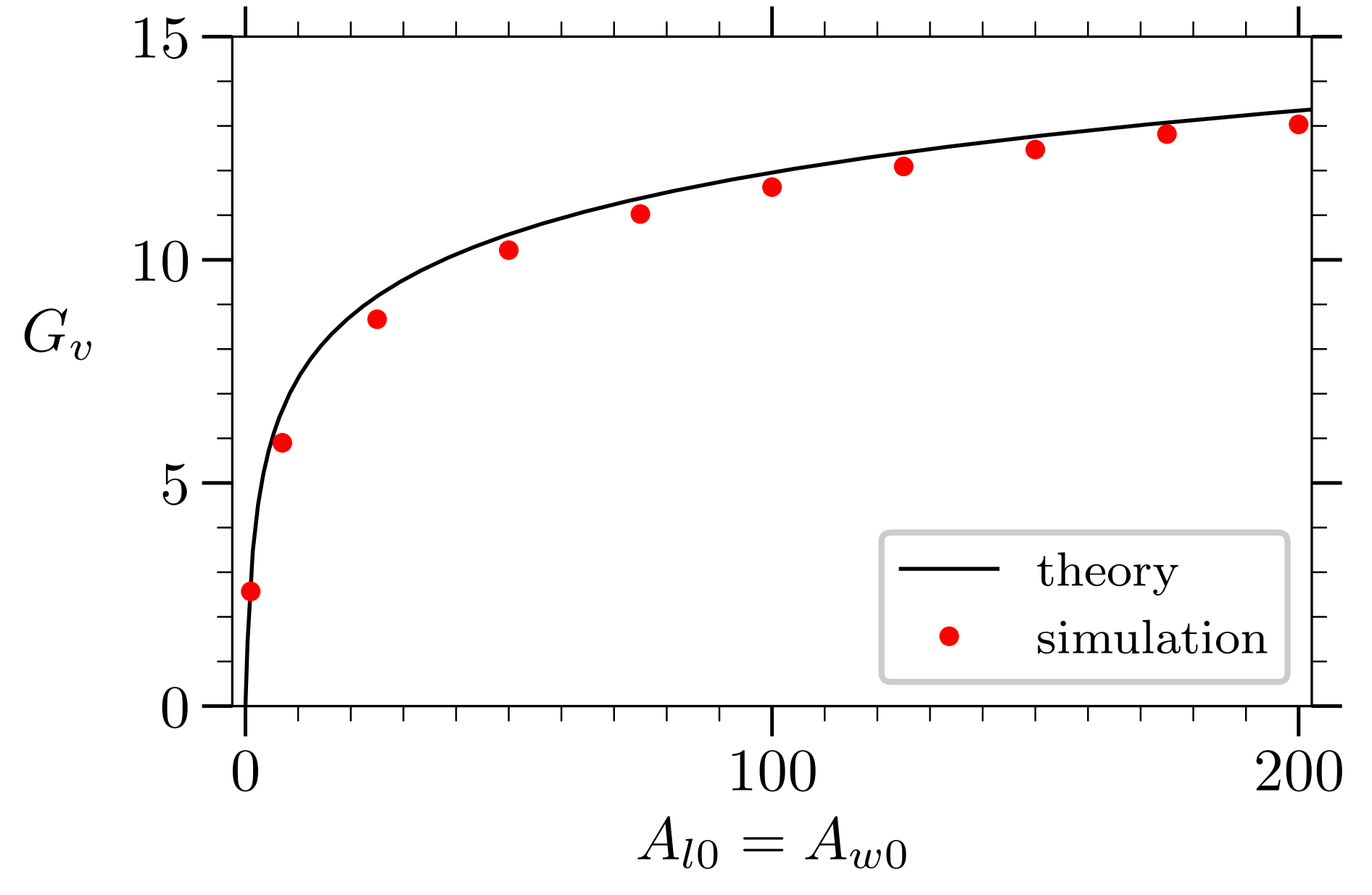
15
10
5
0
G_v
0
100
200
$A_{l0} = A_{w0}$
theory
simulation

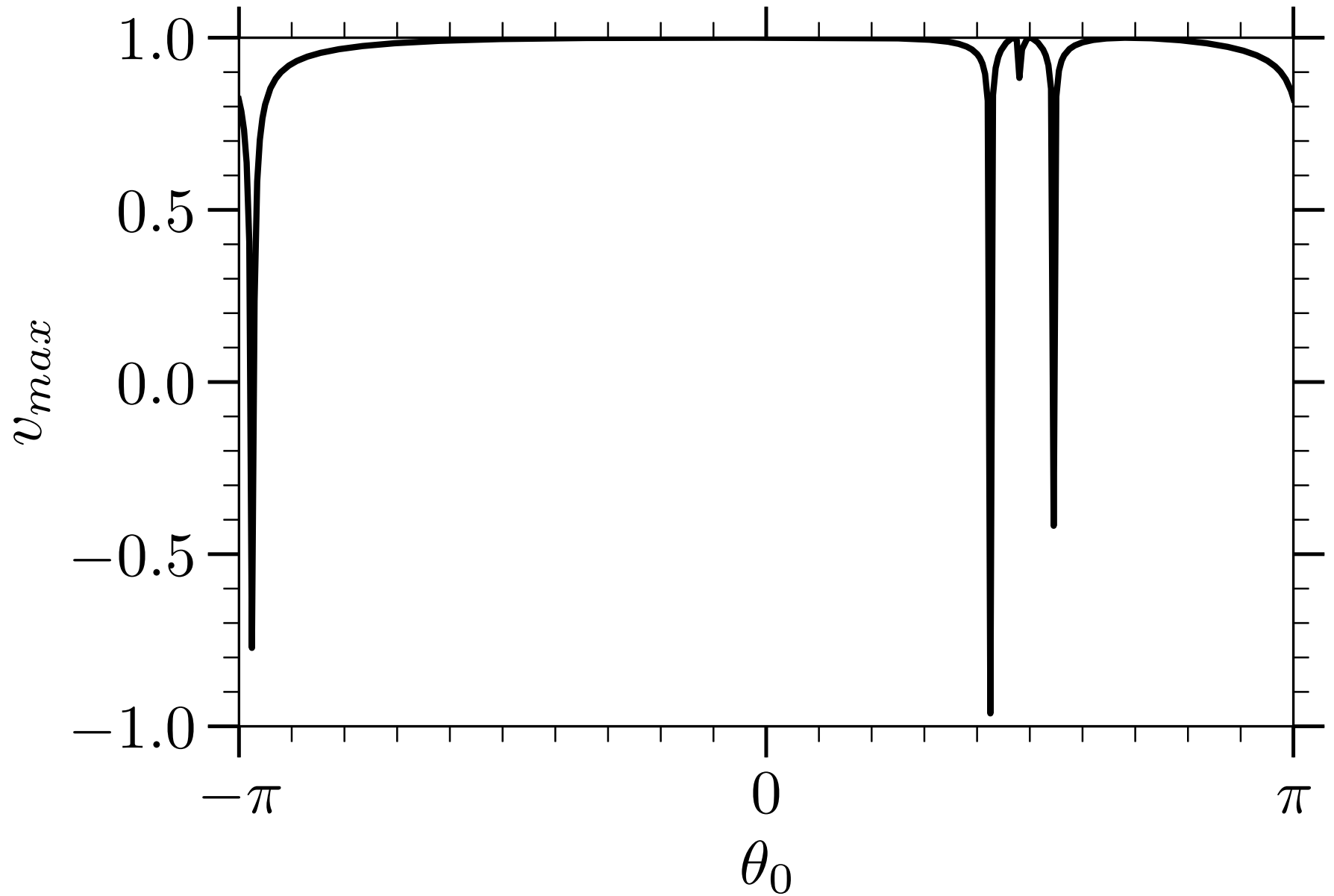
1.0
0.5
0.0
−0.5
−1.0
v_{max}
$-\pi$
0
π
θ_0

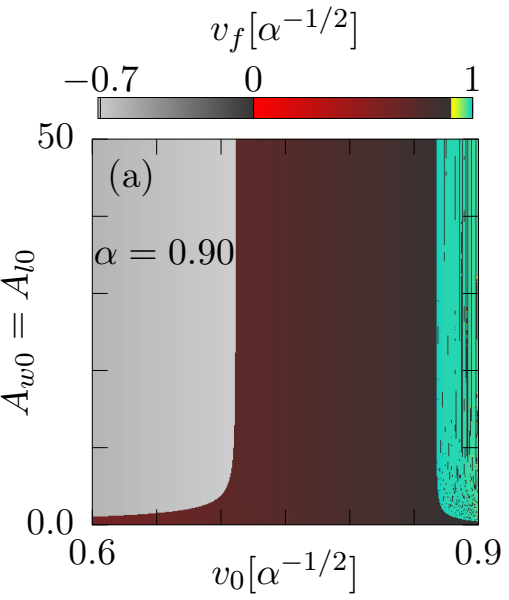
$v_f[\alpha^{-1/2}]$
−0.7
0
1
50
(a)
$\alpha = 0.90$
$A_{w0} = A_{l0}$
0.0
0.6
0.9
$v_0[\alpha^{-1/2}]$

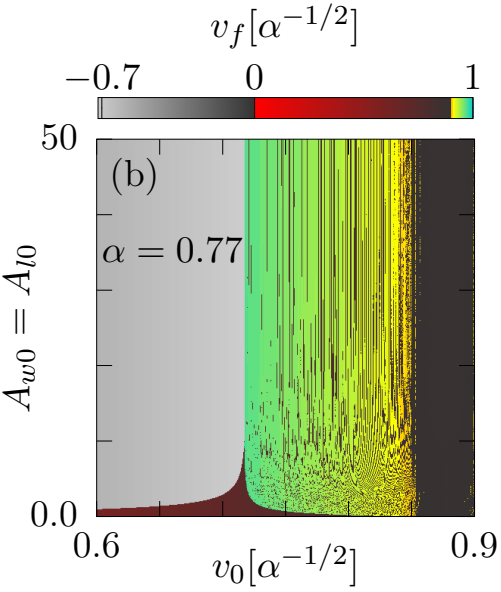
$v_f[\alpha^{-1/2}]$
−0.7
0
1
50
(b)
$\alpha = 0.77$
$A_{w0} = A_{l0}$
0.0
0.6
0.9
$v_0[\alpha^{-1/2}]$

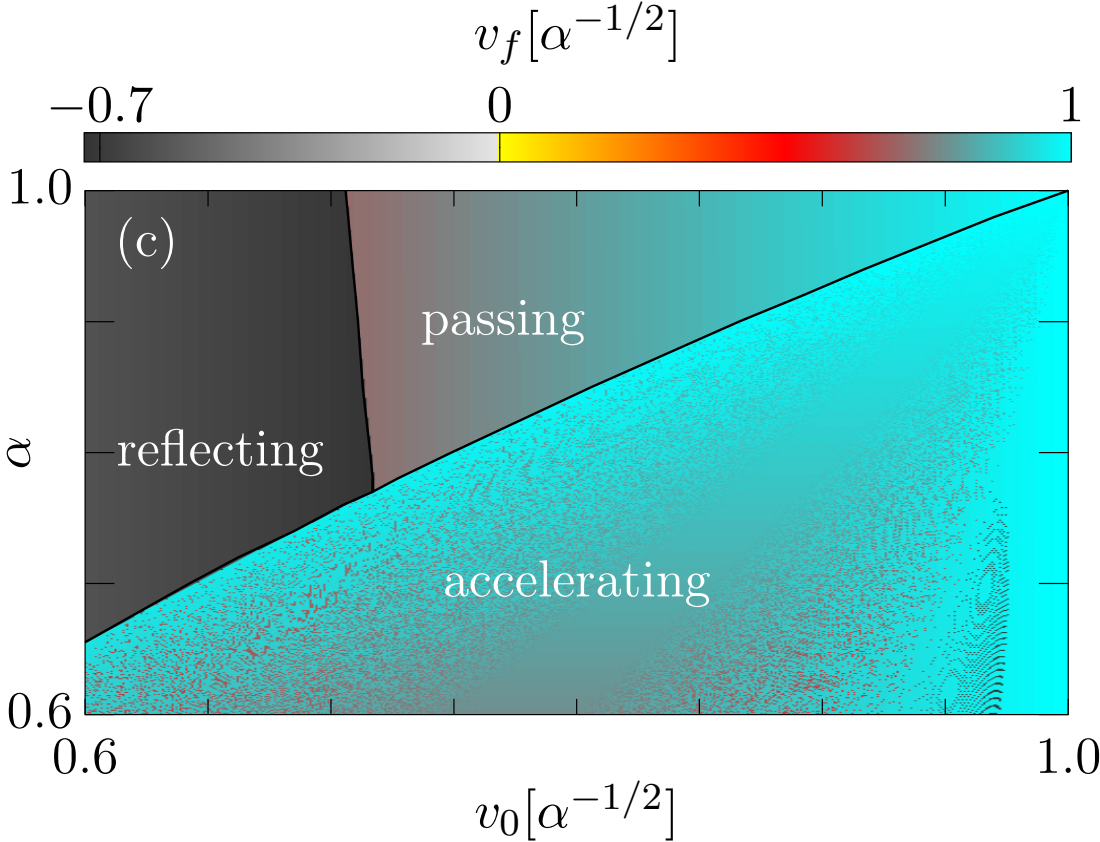
$v_f[\alpha^{-1/2}]$
−0.7
0
1
1.0
(c)
passing
reflecting
α
accelerating
0.6
0.6
1.0
$v_0[\alpha^{-1/2}]$